

Regolith dynamics on small bodies in the Solar System

Kumar Gaurav^{1,*}, Ishan Sharma^{1,2,**}, and Deepayan Banik^{3,***}

¹Department of Mechanical Engineering

²Department of SPASE: Space, Planetary & Astronomical Sciences and Engineering
Indian Institute of Technology Kanpur, Kanpur, UP, India

³Department of Physics, University of Toronto, Canada

Abstract. Many small bodies in the Solar System, such as near-Earth asteroids, are believed to be granular aggregates - *rubble piles* – held together mainly by low self-gravity, typically of the order of mm s^{-2} . Over their lifetime, the evolution of the spin state and shape of such bodies, as well as their bulk and surface differentiation, is affected by numerous geophysical processes that includes radiation, tides, impact cratering, surface activity, thermal cycling, degassing and electromagnetic forces. An ultimate goal is the development of a model that incorporates these processes and is able to follow the body’s development over its lifetime. Here, as a first step, we present a stochastic continuum model to investigate regolith dynamics on small rubble bodies, and its role in the rotational dynamics and reshaping of these bodies. We account for radiation torque and impact-induced landsliding, and couple the body’s rotation to its shape variations. We apply our model to investigate the shape and spin changes of a rubble asteroid over millions of years. An important finding is that the asteroid’s long-term dynamics appears to be controlled by global landsliding events, which has generally been ignored.

1 Introduction

It is generally believed that many asteroids – particularly near-Earth asteroids (NEAs) – are rubble-piles: granular aggregates held together primarily by self-gravity [1, 2]. For example, the irregularly shaped asteroid Itokawa shown in Fig. 1 has a markedly granular surface with smooth valleys and rocky peaks. These objects are meters to several kilometers in size, and it is remarkable that their very low self-gravity keeps them together; e.g. gravity on Itokawa is 0.1 mm s^{-2} !

The life-time evolution of the shape, surface morphology and rotation (or spin) state of these objects is affected by many processes, including impact cratering, seismic shaking, landsliding, thermal cycling, radiation pressure¹ – the Yarkovsky effect [3, 4], radiation torques — the Yarkovsky-O’Keefe-Radzievskii-Paddack (YORP) effect [5–7], tidal events, degassing, orbital changes, rotational dynamics, electromagnetic levitation, and disruptive col-

lisions with other asteroids. Both Yarkovsky effect and YORP torques arise because a body absorbs Solar radiation and emits – through reflection and re-radiation – in different amounts and/or directions. The difference in amounts occurs because the absorption and re-radiation may occur at differing temperatures and, hence, spectra. The change in direction is a direct result of the body’s orbital motion around the Sun and rotation about its own axis. The difference in incoming and outgoing radiation translates into a net pressure and torque on the body, because photons carry both energy and momentum.

All the aforementioned processes may be distinguished as *bulk processes*, wherein the entire body deforms, or *surface processes*, which involve significant motion of only the *regolith* – grains on or just below the surface – but, may itself be initiated by bulk activity, such as seismic shaking. Our broad focus here are surface processes. This is motivated by increasing evidence of loose superficial granular material [8, 9], which necessitates a closer study of regolith motion on asteroids. We emphasize that such a study will encompass investigations into important questions about the response of granular materials in microgravity under various loading conditions. For example, modeling impact-induced landsliding on a spinning rubble asteroid requires, at a minimum, an understanding of how seismic waves spread through a small granular aggregate, how these waves initiate failure of surface granular heaps due to seismic activity and, finally, how granular flow over rough (and rotating) topography takes place. We elaborate on this below.

*e-mail: kugaurav@iitk.ac.in

**e-mail: ishans@iitk.ac.in

***e-mail: deepayan.banik@mail.utoronto.ca

¹All bodies exposed to the Sun experience radiation pressure because they absorb and re-radiate solar photons, which carry both energy and momentum. The manner in which a planetary body is affected by radiation pressure depends upon the body’s thermal inertia, its orbital motion about the Sun and its rigid body rotation. Thermal inertia introduces a delay between absorption and re-radiation, in which time the body moves to a different place in its orbit and rotation reorients the surface previously heated by the Sun. Thus, in general, the body re-radiates from a changed spatial location and in a different direction. The Yarkovsky effect describes how radiation pressure influences the body’s orbital motion. The YORP torque is the integrated moment of the radiation forces about the planetary body’s mass center that affects its rotational dynamics.

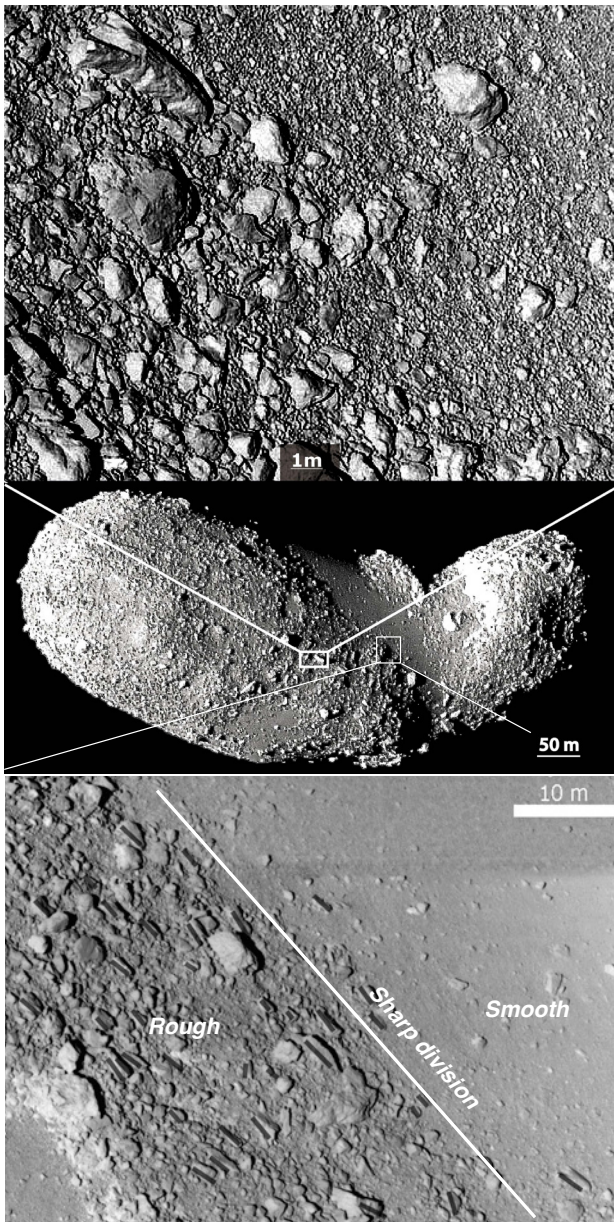


Figure 1. Very high resolution images (top, bottom) of the asteroid Itokawa’s surface (middle). The rubble nature and rough-smooth texturing of the surface is striking. Image: JAXA.

The various surface processes and the evolution of the asteroid’s shape, surface and spin state are generally coupled. For example, Fig. 2 illustrates how collisional activity, YORP, Yarkovsky effect and landslides relate with each other and couple to modifications in the asteroid’s orbit, shape, surface and rotation state. Radiation torques may spin up an asteroid and the elevated rotational accelerations may then allow regolith to be more easily mobilized leading to landsliding events. Subsequently, landslides may rearrange the body’s shape and modify its moment of inertia (MOI) and gravity field. The former modification will affect the rotational dynamics, and may even dominate the action of YORP [10], while the latter will regulate surface grain movement. At the same time, seismic reverberations following non-disruptive collisions may also

release landslides. Surface texturing may be produced in the presence of boulders or grains of differing size and/or density by these reverberations, through mechanisms like the Brazil-nut effect (e.g. [11, 12]), as well as from kinetic sieving [13] that occurs in landslides. Impact cratering will also alter surface features, but will compete with landslides which tend to erase craters [14, 15]. Thus, the most complete model for lifetime evolution of an asteroid due to surface activity must necessarily couple multiple processes that may act across multiple scales. Moreover, the modeling must also be stochastic to reflect our overall ignorance of when the asteroid formed, the environment through its lifetime and the various parameters associated with the active physical processes. The present work constitutes a step towards producing one such framework.

We limit ourselves to coupling impact-induced landsliding and YORP while accounting for changes in the asteroid’s rotation and shape over its lifetime. Our choice is driven by the fact that these processes will be active on all asteroids, even as not all of them may suffer large or disruptive collisions, at least over several millions of years, or experience tidal interactions. Nonetheless, even within these choices there are separate lines of enquiry, each requiring significant work, viz. (a) impact cratering on small rubble-pile bodies, (b) spread of energy post-impact across the body through seismic waves, (c) landslide initiation due to local or global seismic shaking, (d) landslide flow over the asteroid’s irregular topography, while accounting for its rotation, (e) segregation during flow and the role of boulders, and (f) development of a stochastic framework that is able to follow the evolution of the surface, shape and spin state of an asteroid over its lifetime due to impact-induced landsliding, even as it undergoes a large number of impact events.

Here, we primarily address items (d) and (f) above. More precisely, we develop a multi-physics stochastic framework to follow the lifetime evolution of an asteroid’s shape and spin state due to *global, axi-symmetric* impact-induced landsliding and YORP. For this, as shown in Fig. 3, we will couple stochastically occurring impact-induced seismic shaking with landsliding events, and incorporate effects of (a) YORP torques, (b) rotational dynamics and (c) shape change. In our implementation, we neglect crater formation, and ignore shattering impacts – a reasonable assumption over a timeframe of several millions of years – and assume a constant semi-major axis. We initially included Yarkovsky effect and corresponding orbital changes, but found that this had minimal consequences on our outcomes and, hence, neglect them here for a simpler presentation. Finally, we will employ our stochastic model to investigate some evolutionary scenarios for rubble asteroids.

Research on rubble-pile asteroids is extensive and is best left to recent excellent reviews [1, 2, 16, 17]. We limit our literature survey to the present work’s focus.

Spin-state evolution. Variations in the rotation rate of asteroids is explained through many mechanisms: moment of inertia changes due to centrifugal deformation with and without mass shedding [18, 19]; tidal flyby induced torques and deformation [20–22]; and YORP torques in-

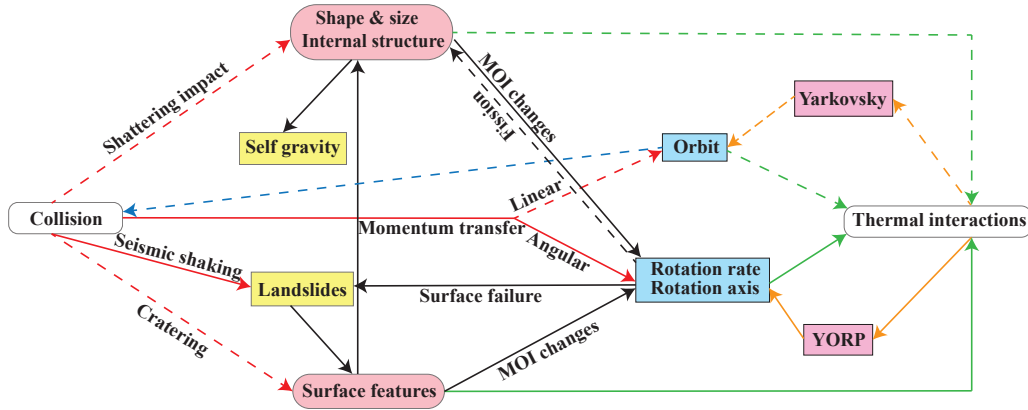


Figure 2. An illustration of how collisional activity, YORP, Yarkovsky effect and landslides are coupled to the asteroid’s orbit, shape, surface and rotation state. Solid arrows indicate connections retained in this study.

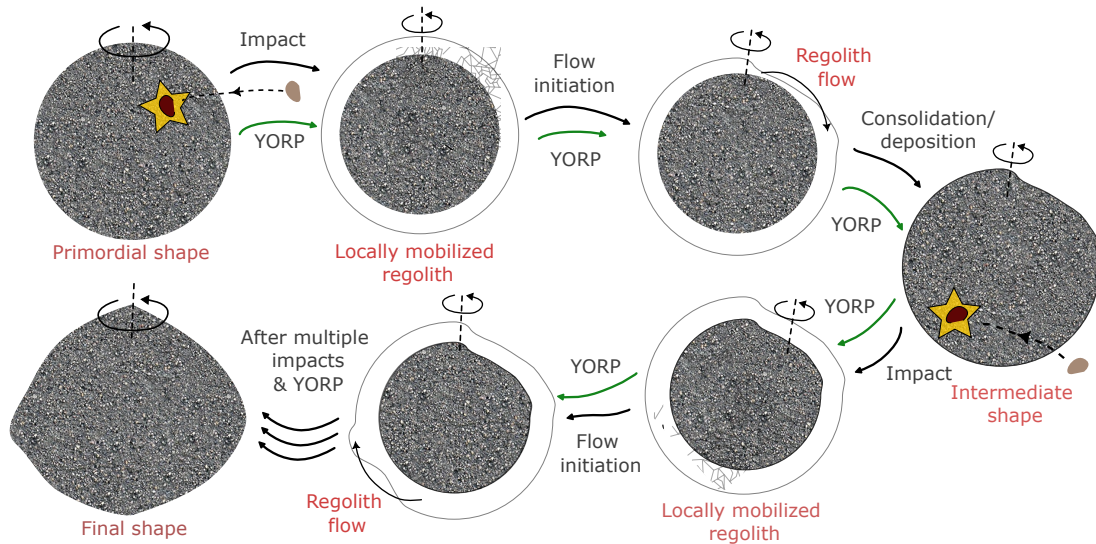


Figure 3. A schematic of our model. The primordial rubble asteroid is affected by YORP torques and experiences many impact events over its lifetime. Impact-induced seismicity mobilizes regolith and may cause landslides that reshape the asteroid. Shape changes and impacts also modify and couple to the asteroid’s rotational dynamics.

dependent of [23, 24] or coupled to [25] the body’s shape evolution. All these mechanisms entail bulk deformation of the asteroid and are mostly studied by the soft-sphere discrete element method (SSDEM) built upon the discrete element method (DEM) of [26]. In contrast, there is little work on how regolith motion on the asteroid’s surface — landsliding — affects the body’s rotation. Multibody dynamics was employed by [27] to study the rotation rate evolution of a rigid asteroid due to motion of rigid surface boulders and their crash and launch events. Recently, [10] coupled modifications in the asteroid’s spin rate to global axisymmetric landslides and consequent shape changes in a continuum framework; but they ignored stochasticity and YORP. The SSDEM simulations of [28] couple rotational dynamics with the effect of an individual landslide, but they too ignore YORP and do not consider multiple landsliding events.

Reshaping. Works on reshaping of rubble-pile asteroids may be distinguished on whether they follow bulk de-

formation or surface processes. Our focus here is the latter, but we quickly mention some representative research in the former domain. Shape changes has been linked to centrifugal effects [18, 19, 23, 29–31], tidal interaction [20] or gravitational re-agglomeration following cataclysmic disruptions [32].

Investigation into surface phenomena that lead to reshaping include launch and crash processes [33–36], cavitation due to local fission [37] and surface failure [38], particle or regolith movement from poles to the equator due to slope instability [39] or landsliding [40, 41] or impact-induced global reverberations [42], debris accumulation onto a rotating solid spherical core [43], an inner solid core’s presence [44], and creeping surface flows [45]. Changes in spin rate, when required, were attributed to YORP torques. However, all works ignored that YORP is critically dependent upon shape [46] and, so, coupled to the shape evolution. Indeed, simulations of [25] report that spin changes induced by YORP and due to modifi-

cations in shape may be comparable. This was supported by [10] in their work on the asteroid Bennu's shape and spin evolution due to multiple impact-induced seismic activity. A major application of the present coupled modeling framework will be to evaluate the relative contributions of YORP and landslides to the shape and spin evolution of rubble asteroids.

Regolith motion. Barring the recent simulations of [28] landsliding on asteroids has not been considered carefully, although elements of this process have been captured in some studies cited above, e.g. [39, 40], or in closely related investigations: [29] explored landslide initiation on spinning spheroidal asteroids, [47] modeled two-dimensional granular flow on a rotating and gravitating ellipse, [48] simulated mass movement near a crater on Bennu, and [49] computed surface motion on the asteroid Apophis during its expected Earth encounter in 2029. At the same time, employing high-resolution images from missions, regolith and boulder motion is being utilized to infer aspects of the body's evolution [9, 48, 50–53]. Thus, there is a clear need for detailed modeling of landslides on small bodies like asteroids.

2 Reshaping & Rotational dynamics

We briefly discuss the processes that affect the evolution of an asteroid over its lifetime in the context of Fig. 3.

1. **Stochastic collisional history.** Because an asteroid faces very many impacts over its lifetime, its evolution must be studied stochastically. To create sample collisional histories requires estimating the distribution of the size, frequency and approach velocity of the impactor, and the manner in which the impacts are spread over the asteroid's surface. For this we extend the Monte Carlo model of [54]. The expected number of impactors with diameter greater than d in a given time period t is

$$\mathbb{E}(N_{>d}^h) = P_i R^2 N_{>d} t, \quad (1)$$

where $P_i \approx 2.8 \times 10^{-18} \text{ km s}^{-2} \text{ yr}^{-1}$ is the intrinsic collisional probability and R is the radius of the target asteroid. We compute the number of impactors in a time interval t using Poisson's distribution with mean $\mathbb{E}(N_{>d}^h)$. The mean impact velocity is set to 5.5 km s^{-1} [55]. The impact on the asteroid's surface is located by its longitude φ and colatitude θ . Assuming the asteroid to be nominally spherical and the impactors to be uniformly distributed around it, we obtain the probability distribution function (PDF) $f(\varphi, \theta)$ of the impact location as $f(\varphi, \theta) = \sin \theta / 4\pi$. Finally, at a given differential surface patch at (φ, θ) and impact speed c , the orientation of the impactor's approach velocity vector \mathbf{c} is described by the vector's tilt Θ from the local surface normal and its azimuth Φ . We may show that Θ and Φ follow the PDF $F(\Theta, \Phi) = \sin \Theta \cos \Theta / \pi$.

2. **Impact-induced seismic shaking and induced regolith failure.** A portion of the impact energy is redistributed as seismic energy through P, S and surface waves. The grains at the surface of a small body are rather loose,

so that we may ignore surface waves. At the same time, our recent DEM simulations suggest that in gently confined granular materials shear motion is converted to longitudinal motion away from the source, because force transfer between grains is primarily along the contact normal. Hence, here we assume that all seismic energy is transferred through P-waves. However, given the complexity of wave transmission through granular media, we follow [12, 15] and estimate the spatio-temporal distribution of the seismic energy density $\epsilon_s(\mathbf{R}, t)$ through the diffusion equation

$$\frac{\partial \epsilon_s}{\partial t} = K_s \nabla^2 \epsilon_s - \frac{2\pi f \epsilon_s}{Q}, \quad (2)$$

where K_s is the seismic diffusivity, Q is the seismic quality factor that estimates the dissipation in the material, and f is the seismic frequency, i.e. the frequency of the seismic wave. We solve the above equation for a spherical body for ϵ_s as a function of time t , location \mathbf{R} and the initial availability of seismic energy at the impact location. We may relate the strength of P waves to ϵ_s by equating seismic energy and strain energy densities.

It remains to associate ϵ_s at a surface location to the amount of regolith that it could cause to fail. For this, we assume that the primary mechanism of failure is that the arrival of a P wave close to the surface reduces the hydrostatic state of stress there in the direction normal to the surface, and this causes the regolith above a critical depth h_f to yield. We thus estimate the change in the principal stresses below the surface due to the P wave by assuming the rubble asteroid material to be incrementally linear elastic, and then find h_f by invoking the Mohr-Coulomb yield criterion [56, Ch. 2]. We obtain

$$h_f = \frac{\sqrt{2\rho\epsilon_p v_p} \tan \delta - c_0}{\rho g (\tan \delta \cos \beta - \sin \beta) + c_1}, \quad (3)$$

where ϵ_p is the peak value of ϵ_s at a location following the arrival of the P wave, v_p is the P wave's speed in regolith, δ is the regolith's friction angle, β is the angle that surface gravity g makes with the local normal, ρ is the regolith's density and $c = c_0 + c_1 h$ its cohesion, which is assumed to increase linearly with the depth h . The latter is prompted the recent impact experiment on the asteroid Ryugu [57] that revealed that the subsurface layers do have cohesive strength. From (3) we observe that below a minimum value $\epsilon_{p,\min}$ of seismic energy there will be no regolith failure. Here we only consider global landslides and, so, must have $\epsilon_p \geq \epsilon_{p,\min}$ everywhere.

3. **Impactor sizes.** An important consideration is the impactors' size range $[d_{\min}, d_{\max}]$, defined by the minimum and maximum impactor diameters. We set $d_{\max} = 0.1d^*$, where d^* is the impactor diameter that results in the catastrophic disruption of a given target. Taking higher values of d_{\max} does not change the collisional history significantly.

The estimate of the minimum impactor diameter d_{\min} required to initiate global landsliding is obtained as follows. From the linearity of (2) we find that, for given seismic parameters, ϵ_p will scale with the impactor's kinetic

energy which, in turn, is proportional to d^3 . Now, for a spherical body, the peak seismic energy density ϵ_p will be minimum at the point diametrically opposite to the impact location. Consequently, from (2) and (3), we find

$$d_{\min} = \left(\frac{\epsilon_{p,\min}}{\epsilon_{p,0}} \right)^{1/3} = \left(\frac{c_0^2}{2\rho\epsilon_0 v_p^2 \tan^2 \delta} \right)^{1/3}, \quad (4)$$

where $\epsilon_{p,0}$ is the peak seismic energy density received at a point diametrically opposite from a meter-sized impactor.

4. Landslides. We extend the approach of [10] that modeled regolith motion on an asteroid, and was itself built upon the methods of [58, 59] that were developed for terrestrial landslides. The asteroid comprises of a regolith layer on a solid central body (CB) representing tightly packed grains; see Fig. 4. The shape and size of CB may change when it interacts with the moving regolith due to erosion and deposition. The comprehensive set of equations governing the coupled motion of the CB and regolith are present in [60], which are then greatly simplified under the following physically motivated assumptions: (a) we take the asteroid's initial shape to be spherical of radius R_0 with a shallow basal topography of thickness $h^b \ll R_0$; (b) the landslides are incompressible and shallow, in that their typical depth h_0 is much smaller than their horizontal spread that is generally of $O(R_0)$; (c) consequently, we ignore the effect of regolith motion and mass shedding upon the displacement of the system's mass center; (d) the basal topography is modified by multiple landslides, so that we take $h^b \gg h_0$; (e) the asteroid is taken to be in pure spin $\omega = \omega \hat{e}_3$, whose magnitude may change, but we ignore any wobble introduced by impacts and mass redistribution by landslides; (f) during a landsliding event, whose duration is much shorter than an asteroid's lifetime, there are no impacts and thermal radiation influences may be disregarded; (g) we limit ourselves to isolated asteroids, so that tidal interactions are absent.

Recall that we limit ourselves to axisymmetric global landslides. Equations for the flow are obtained by invoking the balances of mass and linear momentum. The flow's incompressibility simplifies mass balance, while its shallowness allows us to reduce the dimensionality of the problem by averaging the balance equations through the landslide's depth along the radial r direction and retaining terms only up to $O(h^b/R_0)$. Note that, because of the shallowness of the landslides, the r direction is approximately normal to the CB's surface. Depth-averaging mass, and linear momentum balances in the θ and ϕ directions will provide three equations for the landslide's depth $h(\theta, t)$ and its depth-averaged velocities \bar{u}_θ and \bar{u}_ϕ in the θ and ϕ directions, respectively. These equations up to $O(h^b/R_0)$ are,

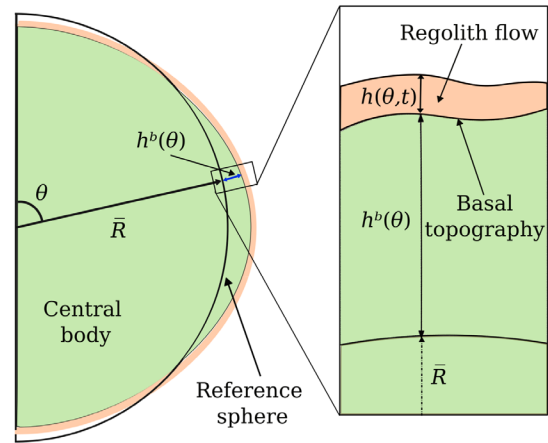
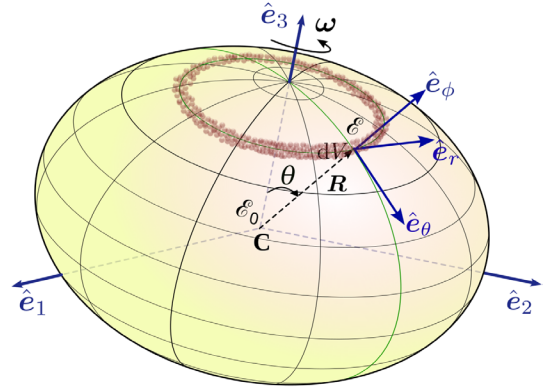


Figure 4. Top: An asteroid rotating at angular velocity ω directed along \hat{e}_3 . Also shown are the body-fixed $\{\mathcal{E}_0, C, \hat{e}_i\}$ and spherical $\{\mathcal{E}, R, \hat{g}_i\}$ coordinate systems, along with the position vector \mathbf{R} of a surface point and a differential axisymmetric volume element dV of a landslide. Bottom: An axisymmetric landslide over the basal topography and the reference sphere.

respectively,

$$\frac{\partial}{\partial t} \{h\lambda^2 \sin \theta\} + \frac{\partial}{\partial \theta} \{\bar{u}_\theta h \lambda \sin \theta\} = 0, \quad (5)$$

$$\begin{aligned} & \frac{\partial}{\partial t} \{\bar{u}_\theta h \lambda^3 \sin \theta\} + \frac{\partial}{\partial \theta} \left\{ \left(\bar{u}_\theta^2 + \psi \frac{h}{2} \right) h \lambda^2 \sin \theta \right\} \\ & = \lambda^3 h \sin \theta \left\{ - \left(\mu \hat{u}_\theta + \frac{\partial h^b}{\partial \theta} \right) \psi + \frac{\bar{u}_\theta^2}{\lambda} \cot \theta \dots \right. \\ & \left. \dots + (b_\theta + 2\bar{u}_\theta \omega \cos \theta + \omega^2 \lambda \sin \theta \cos \theta) \right\} \end{aligned} \quad (6)$$

$$\begin{aligned} \text{and} \quad & \frac{\partial}{\partial t} \{\bar{u}_\phi h \lambda^3 \sin^2 \theta\} + \frac{\partial}{\partial \theta} \{\bar{u}_\phi \bar{u}_\theta h \lambda^2 \sin^2 \theta\} \\ & = - \left\{ \mu \hat{u}_\phi \psi + 2\omega \bar{u}_\theta \cos \theta \right\} \lambda^3 h \sin^2 \theta, \end{aligned} \quad (7)$$

where, as shown in Fig. 4, $h(\theta, t)$ is the height of the regolith flow's free surface above the basal surface that is, in turn, identified as the CB's outer surface, $\lambda = \bar{R} + h^b(\theta)$ is the radial distance of the basal surface from body's center in terms of the mean radius \bar{R} of the reference sphere and the deviation h^b of the CB from it,

$$\psi = - \left\{ \left(\frac{\bar{u}_\theta^2 + \bar{u}_\phi^2}{\lambda} \right) + \bar{b}_r + \omega^2 \sin^2 \theta + 2\bar{u}_\phi \omega \sin \theta \right\} \quad (8)$$

estimates the net basal pressure, \bar{b}_θ and \bar{b}_r are the components of gravity along θ and r directions, $\mu = \tan \delta$ is the basal friction coefficient and $\hat{u}_i = \bar{u}_i / \sqrt{(\bar{u}_\theta)^2 + (\bar{u}_\phi)^2}$, with $i = \theta$ or ϕ . Note that the boundary conditions at the landslide's top and bottom surfaces get included during depth averaging. The top surface is free, while the forces at the bottom are modeled through a Coulomb-like basal friction law relating normal pressure and shear traction.

The angular momentum balance (AMB) of the system up to $O(h^b/R_0)$ provides the angular acceleration:

$$\alpha = \dot{\omega} = \frac{1}{C} \left\{ \int_0^\pi \mu \hat{u}_\phi \psi \lambda^3 h \sin^2 \theta \, d\theta - \dot{H}_s \right\} \quad (9)$$

where $C = \frac{4}{15} \left(1 + \frac{15}{4} \int_0^\pi \gamma h^b \sin^3 \theta \, d\theta \right)$

is the CB's moment of inertia about its principal axis and \dot{H}_s is the rate at which angular momentum is lost due to mass shedding. The AMB (9) provides α in terms of \bar{u}_ϕ and the landslide's depth h . Further, the AMB reveals that, in the absence of external torque, the CB's angular momentum is modified solely by interaction with the flowing regolith – the integral in (9) is the total torque from basal shear in the ϕ -direction.

We now make two remarks. First, we follow [47] and assume that mass is shed when basal pressure becomes negative, and this is approximated by

$$P_{rr} = \left(1 - \gamma \mu \hat{u}_\theta \frac{dh^b}{d\theta} \right) \psi h < 0,$$

where ψ is given by (8). Second, we may determine the change $\delta\omega$ in the asteroid's rotation rate due to regolith flow and mass shedding by integrating (9) over the duration t_f of the landslide to find

$$\delta\omega = -\frac{\omega_0}{C} \left(\left[\int_0^\pi h \lambda^4 \sin^3 \theta \, d\theta \right]_{t=0}^{t=t_f} + \int_0^{t_f} \dot{H}_s dt \right), \quad (10)$$

where ω_0 is the angular velocity of the primordial asteroid.

5. Model summary, parameters & computations. Following an impact, the depth of failed regolith is given by (3). To keep our analysis axisymmetric, we assume that a uniform layer of regolith fails everywhere, whose total mass equals that computed from (3). Subsequently, this mobilized regolith layer flows and its depth h , and flow velocities \bar{u}_θ and \bar{u}_ϕ are found from (5) – (7). We do not account for erosion or deposition of material during this landsliding. Once the landslide stops, the flowing layer consolidates onto the asteroid's surface, merging with the CB, thereby changing $h^b(\theta)$ and modifying the asteroid's shape. At the same time, the asteroid's spin is altered by $\delta\omega$ found from (10). Subsequent impacts repeat the process, as shown in Fig. 3, with the number of impactors, impact time, impactor size, momentum and approach velocity, and the impact location on the asteroid's surface all being distributed stochastically. Finally, throughout its life YORP continues to affect the asteroid's rotation rate. Recall that here we ignore change in the rotation axis –

which is generally found to be small – and follow only the rotation rate. The flowchart of the computational implementation our model is provided in Fig. 5.

Selection of the various parameters entering into the model is challenging, because not much is known about small extraterrestrial bodies. We briefly describe our methodology.

(a) *P wave speed (v_p):* Wave speeds in asteroid regolith are not known. Measurements during Apollo missions reported [61] the average P wave speed in lunar regolith of thickness 8.5 m to be $v_p^D \approx 100 \text{ m s}^{-1}$. We now follow [62] and take v_p to vary with pressure as $p^{1/4}$. Then, assuming pressure to be hydrostatic, i.e. $p \approx \rho gh$, yields $v_p \propto g^{1/4}$, where g is the gravity. This allows us to estimate P wave speed in a rubble asteroid from

$$v_p = v_p^D (g/g^D)^{1/4}. \quad (11)$$

(b) *Seismic parameters:* Seismic waves contain energy at various frequencies. However, only low-frequency waves are able travel long distances as high-frequency modes decay rapidly. The seismic frequency f depends upon impact duration, with longer impacts contributing to the low-frequency power spectrum. Now, the impact duration depends inversely on v_p [42]. Lunar experiments report peak seismic frequencies between 5 – 30 Hz [15]. Because from (11) we find that v_p for sub-kilometer size asteroids is an order smaller than v_p^D , we assume a lower $f = 1 \text{ Hz}$. Next, following [15], we take the seismic quality factor $Q = 1500$ and the seismic efficiency factor $\eta = 10^{-6}$. Finally, the seismic diffusivity $K_s = v_p l_s / 3$, where l_s is the mean free path for the scattering of seismic waves; [15] utilized $l_s = 250 \text{ m}$ and [12] set it equal to the mean asteroid diameter. In a rubble pile we expect more scattering and, so, fix $l_s = 100 \text{ m}$.

(c) *Regolith properties:* The regolith's static and dynamic friction angles are taken to be, respectively, 35° and 25° ; the former controls the regolith's failure and the latter regulates its flow. As surface regolith is nearly cohesionless we take $c_0 = 0.1 \text{ Pa}$, but set $c_1 = 1 \text{ Pa s}^{-1}$

3 Results & Discussion

We now discuss the outcomes of our model in the context of a few indicative examples. We consider an asteroid with mean diameter $D = 500 \text{ m}$ on an orbit with semi-major axis $e = 2.3 \text{ AU}$ and density $\rho = 1250 \text{ kg m}^{-3}$. From (11) we estimate a P wave speed of $v_p = 10 \text{ m s}^{-1}$. For simplicity, the impactor velocities are set at $v_i = 5.5 \text{ km s}^{-1}$.

Figure 6 reports evolution in a rubble asteroid's rotation period due to landslides (L), YORP torque (Y) and collisions (C) for various combinations. In each case we perform 10 simulations and report their mean. The asteroid was initially spinning slowly. We assume a YORP torque that consistently increases the rotation rate, because observations [63] report that NEAs spin up over time. Figure 6 shows that collisions have a negligible effect on spin over 0.5 million years (Myrs). This was expected as most

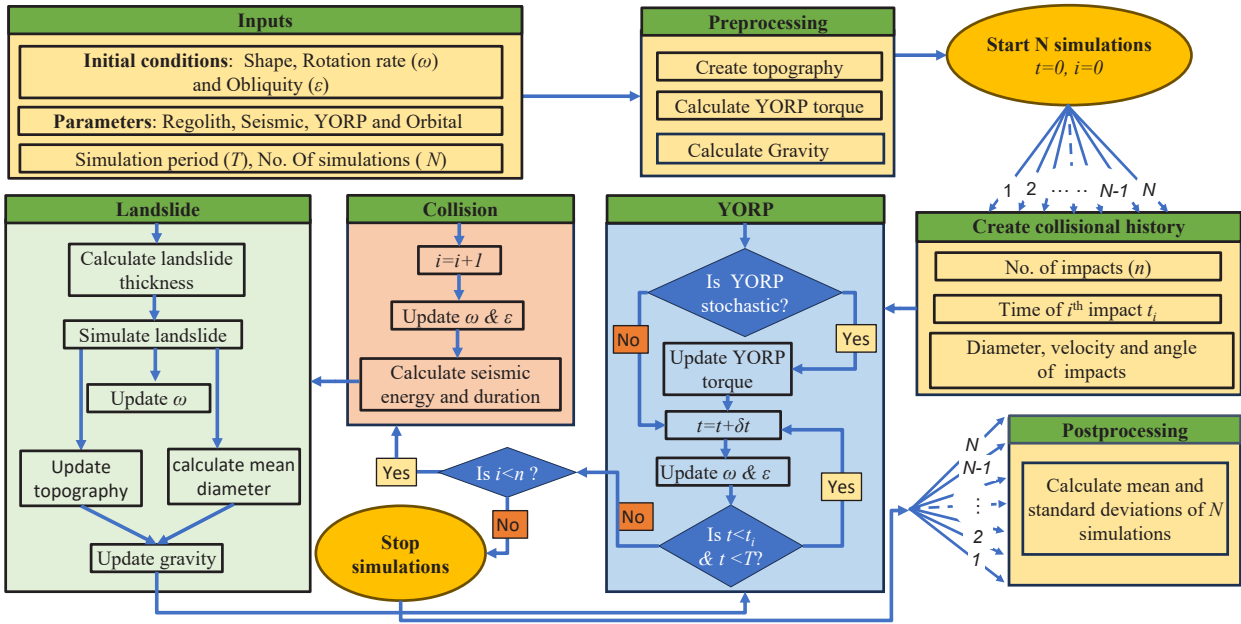


Figure 5. The flowchart of our computational model. More details are available in [60].

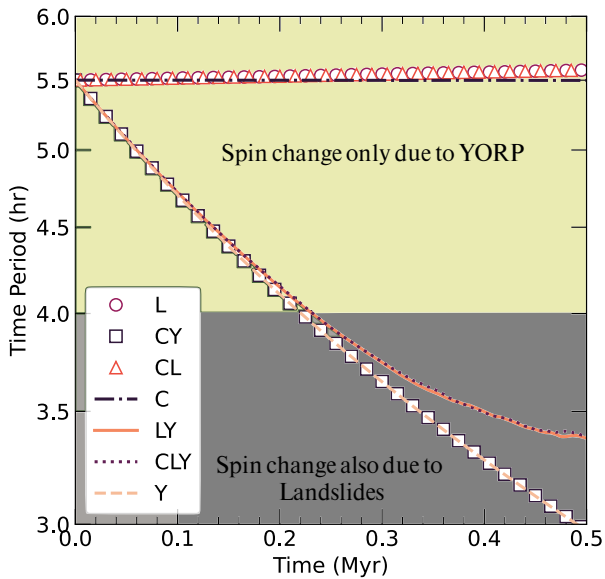


Figure 6. Evolution of the time period of an initially spherical asteroid over 0.5 Myr in presence of one or more of the following mechanisms: collisions (C), landslides (L) and YORP torques (Y); thus, CLY indicates that all three mechanisms are active.

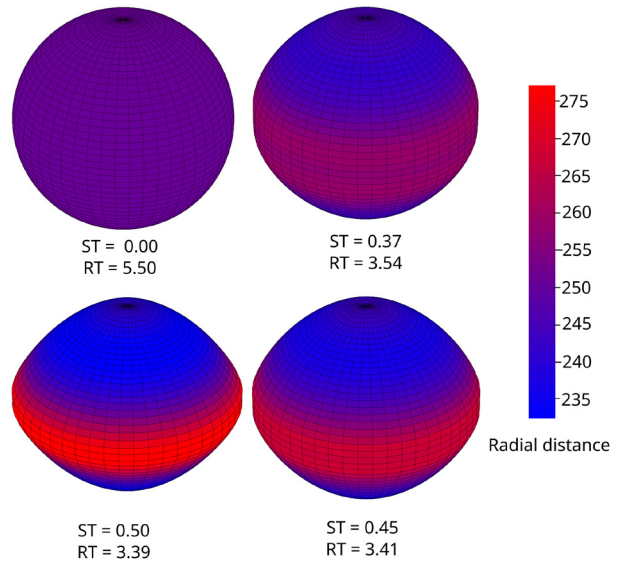


Figure 7. Continued from Fig. 6. Evolution of the shape of the asteroid that follows the CLY curve in Fig. 6. Radial distance is measured from the body’s center, ST is simulation time and RT is the rotational time period.

impactors were small. Furthermore, the collisional parameters were statistically distributed, and the small impactors were numerous enough, so that the spin change introduced by collisions averaged out over time.

We find from Fig. 6 that the primary factors affecting spin are YORP and landslides. On their own, landslides redistribute surface regolith towards the equator, thereby raising the asteroid’s moment of inertia and, consequently, lowering its rotation rate in order to conserve the system’s

angular momentum. However, landsliding effects are observed to be minimal at slow rotation rates, but become progressively dominant as the asteroid spins faster. This is explained below when we discuss shape changes.

We consider spin evolution in the presence of all mechanisms, as depicted by the CLY curve in Fig. 6. We find that the rotation period saturates at about 3.4 hrs. Thus, rotational fission – that occurs at a period of 2.95 hrs – will not happen, in contrast to when landslides are ignored

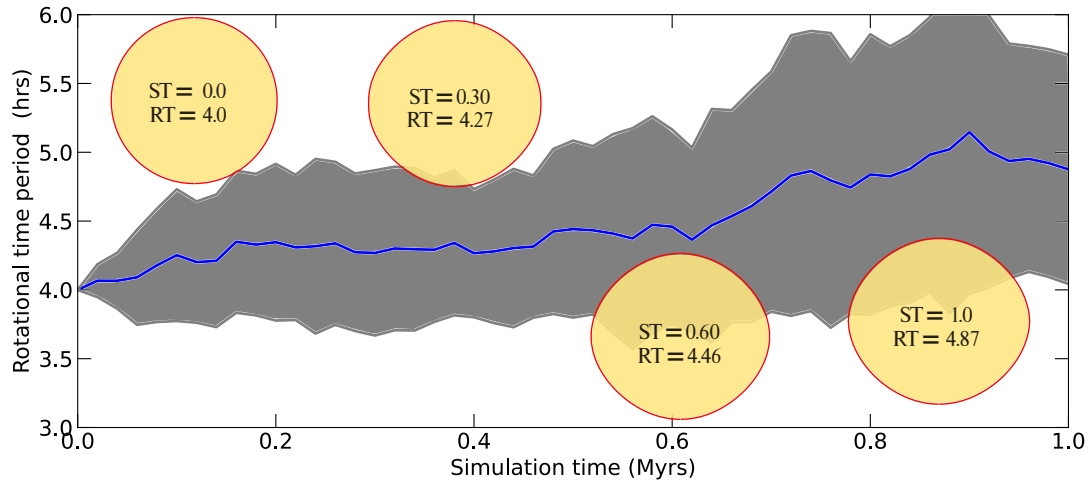


Figure 8. Evolution of the mean shape and the mean spin in the presence of stochastic YORP. The shaded region in gray depicts the standard deviation of 10 simulations. As in Fig. 7, ST is the simulation time and RT is the rotational time period.

and YORP is allowed to continuously spin up the body; see the CY or Y curves in Fig. 6. We may then conclude that YORP governs the spin evolution of small slow rotators, while landslides become dominant once the body’s rotation is fast enough, thereby controlling the final outcome. Indeed, we observe in Fig. 6 that the curves Y, CY, LY, and CLY all remain together until the rotation period drops to around 4 hour. Once the body rotates faster than this, the Y and CY curves depart together from the LY and CLY curves and continue their original trajectory. In contrast, the LY and CLY curves appear to plateau because of reshaping by landslides.

The above observation is reinforced when we consider in Fig. 7 how the asteroid’s shape changes as it evolves along the CLY curve in Fig. 6. Recall that our model presently ignores reshaping due to impacts. During land-sliding events tangential components of gravitational and centrifugal forces move the regolith towards the equator, forming an equatorial bulge and creating a “top” shape. This augments the body’s moment of inertia which, in turn, lowers its spin in competition with the YORP torque that raises the rotation rate. When YORP wins, the body spins up. This accelerates bulge formation as (a) the lower normal gravity in a top-shaped body and the increased centrifugal force reduce the basal pressure and, hence, the basal resistance, and (b) the equator-bound flow is made stronger by the increased centrifugal force.

Above, we assumed that YORP torque always spins up the asteroid. However, YORP is very sensitive to modifications in surface features [46]. Thus, we now investigate a scenario where the YORP torque is stochastic, in that the sign and magnitude of the torque resets after each land-sliding event. Consequently, the body experiences periods of both spin-up and spin-down. Figure 8 reports the outcome for an asteroid initially spinning faster than in Fig. 6. We find that the mean rotation period now *increases* slowly with time and the spin evolution is controlled by land-sliding. Because the asteroid spins down, the shape change in Fig. 8 is less prominent than in Fig. 7 and the formation

of top shape is also delayed. In fact, there are parameter regimes where top shapes emerge after timescales that are longer than the expected lifespan of NEAs.

From the examples above we hypothesize that, while a rubble asteroid may spin up due to YORP over a time scale of a few thousand years, it will ultimately slow down over millions of years due to reshaping by impact-induced landslides, which also explain the commonly observed top shapes. Moreover, rubble bodies will generally not undergo rotational fission.

4 Outlook

The work here is a step towards investigating the dynamical evolution of small granular bodies in the Solar System over their lifetimes. Implementing a stochastic continuum model allowed us to follow the changes in the shape and spin a rubble asteroid over millions of years due to regolith motion coupled to the body’s rotational dynamics and influenced by radiation torques and impact-induced land-sliding. This would not be possible through more direct techniques like discrete element simulations that are very computationally intensive.

Nevertheless, as detailed in Sec. 1, many important and challenging improvements need to be made both in computational techniques and in the physical modeling of granular aggregates in a rotating, low-gravity environment, in the presence of collisions and interactions with other bodies. Presently we aim to firm up our conclusions above by surveying a wide range of physical parameters and, then, relax the strong assumption of landslides being global and axisymmetric. For the latter, a first attempt from Gaurav & Sharma is included in these proceedings. This will be accompanied by extending our model’s capabilities to handle regolith comprised of different types of grains to study surface texturing on asteroids, for which we will employ mixture theory, as did [47]. In this context, see Nallani *et al.* in these proceedings who present a hypothesis to explain segregation on Itokawa shown in Fig. 1.

Finally, given the importance that boulders are playing in revealing the geological history of small bodies [51–53], we plan also to incorporate the entrainment and presence of boulders in regolith flow.

References

- [1] K.J. Walsh, Rubble pile asteroids, *Annu. Rev. Astron. Astrophys.* **56**, 593 (2018).
- [2] D. Hestroffer, and 14 others, Small solar system bodies as granular media, *Astron. Astrophys. Rev.* **27**, 1 (2019).
- [3] E.J. Öpik, Collision probabilities with the planets and the distribution of interplanetary matter, *Proc. R. I. Acad. A., Math. Phys. Sci.* **54**, 165 (1951).
- [4] D. Vokrouhlický, W.F. Bottke Jr., S.R. Chesley, D.J. Scheeres, T.S. Statler, in *Asteroids IV*, edited by P. Michel, F.E. DeMeo, W.F. Bottke Jr. (U. Arizona Press, Tucson, AZ, 2015), pp. 509–531
- [5] V.V. Radzievskii, About the influence of the anisotropically reemitted solar radiation on the orbits of asteroids and meteoroids, *Astron. Zh.* **29**, 162 (1952).
- [6] V.V. Radzievskii, A mechanism for the disintegration of asteroids and meteorites, *Dokl. Akad. Nauk SSSR* **97**, 49 (1954).
- [7] D.P. Rubincam, Radiative spin-up and spin-down of small asteroids, *Icarus* **148**, 2 (2000).
- [8] N. Murdoch, P. Sánchez, S.R. Schwartz, H. Miyamoto, in *Asteroids IV*, edited by P. Michel, F.E. DeMeo, W.F. Bottke Jr. (U. Arizona Press, Tucson, AZ, 2015), pp. 767–92
- [9] E.R. Jawin, and 20 others, Global patterns of recent mass movement on asteroid (101955) Bennu, *J. Geophys. Res. Planets* **125**, e2020JE006475 (2020).
- [10] D. Banik, K. Gaurav, I. Sharma, Regolith flow on top-shaped asteroids, *Proc. R. Soc. A* **478**, 20210972 (2022).
- [11] A. Rosato, K.J. Strandburg, F. Prinz, R.H. Swendsen, Why the Brazil nuts are on top: Size segregation of particulate matter by shaking, *Phys. Rev. Lett.* **58**, 1038 (1987).
- [12] S. Ghosh, I. Sharma, D. Dhingra, Segregation on small rubble bodies due to impact-induced seismic shaking, *Proc. Royal Soc. A* **480**, 20230715 (2024).
- [13] J.W. Vallance, S.B. Savage, Particle segregation in granular flows down chutes, in *IUTAM Symposium on Segregation in Granular Flows: Proceedings of the IUTAM Symposium held in Cape May, NJ, USA June 5–10, 1999* (Springer, 2000), pp. 31–51
- [14] J.E. Richardson Jr., H.J. Melosh, R. Greenberg, Impact-induced seismic activity on asteroid 433 Eros: A surface modification process, *Science* **306**, 1526 (2004).
- [15] J.E. Richardson Jr., H.J. Melosh, R. Greenberg, D.P. O’Brien, The global effects of impact-induced seismic activity on fractured asteroid surface morphology, *Icarus* **179**, 325 (2005).
- [16] P. Michel, F.E. DeMeo, W.F. Bottke Jr., *Asteroids IV* (U. Arizona Press, Tucson, AZ, 2015)
- [17] Y. Zhang, P. Michel, Shapes, structures, and evolution of small bodies, *Astrodynamics* **5**, 293 (2021).
- [18] I. Sharma, J.T. Jenkins, J.A. Burns, Dynamical passage to approximate equilibrium shapes for spinning, gravitating rubble asteroids, *Icarus* **200**, 304 (2009).
- [19] K.J. Walsh, D.C. Richardson, P. Michel, Spin-up of rubble-pile asteroids: Disruption, satellite formation, and equilibrium shapes, *Icarus* **220**, 514 (2012).
- [20] I. Sharma, J.T. Jenkins, J.A. Burns, Tidal encounters of ellipsoidal granular asteroids with planets, *Icarus* **183**, 312 (2006).
- [21] Y. Zhang, P. Michel, Tidal distortion and disruption of rubble-pile bodies revisited- soft-sphere discrete element analyses, *Astron. Astrophys.* **640**, A102 (2020).
- [22] A.V. Melnikov, Rotational dynamics of asteroids approaching planets, *Sol. Syst. Res.* **56**, 241 (2022).
- [23] K.J. Walsh, D.C. Richardson, P. Michel, Rotational breakup as the origin of small binary asteroids, *Nature* **454**, 188 (2008).
- [24] M. Kanamaru, 14 others, YORP effect on asteroid 162173 ryugu: implications for the dynamical history, *J. Geophys. Res. Planets* **126**, e2021JE006863 (2021).
- [25] D. Cotto-Figueroa, T.S. Statler, D.C. Richardson, P. Tanga, Coupled spin and shape evolution of small rubble-pile asteroids: Self-limitation of the YORP effect, *Astrophys. J.* **803**, 25 (2015).
- [26] P.A. Cundall, O.D.L. Strack, A discrete numerical model for granular assemblies, *Géotechnique* **29**, 47 (1979).
- [27] D.N. Brack, J.W. McMahon, Modeling the coupled dynamics of an asteroid with surface boulder motion, *Icarus* **333**, 96 (2019).
- [28] Z. Song, Y. Yu, S. Soldini, B. Cheng, P. Michel, An integrated dem code for tracing the entire regolith mass movement on asteroids, *Mont. Not. R. Astron. Soc.* **532**, 1307 (2024).
- [29] D.J. Scheeres, Landslides and mass shedding on spinning spheroidal asteroids, *Icarus* **247**, 1 (2015).
- [30] D.J. Scheeres, 40 others, and The OSIRIS-REx Team, The dynamic geophysical environment of (101955) Bennu based on OSIRIS-REx measurements, *Nat. Astron.* **3**, 352 (2019).
- [31] M. Hirabayashi, D.J. Scheeres, Rotationally induced failure of irregularly shaped asteroids, *Icarus* **317**, 354 (2019).
- [32] P. Michel, and 14 others, Collisional formation of top-shaped asteroids and implications for the origins of Ryugu and Bennu, *Nat. Commun.* **11**, 1 (2020).
- [33] Y. Yu, P. Michel, M. Hirabayashi, S.R. Schwartz, Y. Zhang, D.C. Richardson, X. Liu, The dynamical complexity of surface mass shedding from a top-shaped asteroid near the critical spin limit, *Astron. J.* **156**, 59 (2018).

- [34] R. Ikeya, N. Hirata, Ejecta emplacement as the possible origin of Ryugu's equatorial ridge, *Icarus* p. 114590 (2021).
- [35] L.D. Vance, J. Thangavelautham, E. Asphaug, D. Cotto-Figueroa, Possible particle ejection contributions to the shape and spin stability of small near-Earth asteroids, *Icarus* **384**, 115078 (2022).
- [36] G. Madeira, S. Charnoz, R. Hyodo, Dynamical origin of Dimorphos from fast spinning Didymos, *Icarus* **394**, 115428 (2023).
- [37] S. Tardivel, P. Sánchez, D.J. Scheeres, Equatorial cavities on asteroids, an evidence of fission events, *Icarus* **304**, 192 (2018).
- [38] M. Hirabayashi, and 16 others, Spin-driven evolution of asteroids' top-shapes at fast and slow spins seen from (101955) Bennu and (162173) Ryugu, *Icarus* **352**, 113946 (2020).
- [39] A.W. Harris, E.G. Fahnestock, P. Pravec, On the shapes and spins of "rubble pile" asteroids, *Icarus* **199**, 310 (2009).
- [40] K. Sugiura, H. Kobayashi, S. Watanabe, H. Genda, R. Hyodo, S. Inutsuka, Sph simulations for shape deformation of rubble-pile asteroids through spinup: The challenge for making top-shaped asteroids Ryugu and Bennu, *Icarus* **365**, 114505 (2021).
- [41] R. Hyodo, K. Sugiura, Formation of moons and equatorial ridge around top-shaped asteroids after surface landslide, *Astrophys. J. Lett.* **937**, L36 (2022).
- [42] A.C. Quillen, Y. Zhao, Y. Chen, P. Sanchez, R.C. Nelson, S.R. Schwartz, Impact excitation of a seismic pulse and vibrational normal modes on asteroid Bennu and associated slumping of regolith, *Icarus* **319**, 312 (2019).
- [43] T. Sabuwala, P. Chakraborty, T. Shinbrot, Bennu and Ryugu: diamonds in the sky, *Granul. Matter* **23**, 1 (2021).
- [44] F. Ferrari, P. Tanga, Interior of top-shaped asteroids with cohesionless surface, *Icarus* **378**, 114914 (2022).
- [45] Y. Zhang, D.C. Richardson, O.S. Barnouin, C. Murel, P. Michel, S.R. Schwartz, R.L. Ballouz, L.A. Benner, S.P. Naidu, J. Li, Creep stability of the proposed AIDA mission target 65803 Didymos: I. Discrete cohesionless granular physics model, *Icarus* **294**, 98 (2017).
- [46] T.S. Statler, Extreme sensitivity of the YORP effect to small-scale topography, *Icarus* **202**, 502 (2009).
- [47] K. Gaurav, D. Banik, I. Sharma, P. Dutt, Granular flow on a rotating and gravitating elliptical body, *J. Fluid Mech.* **916** (2021).
- [48] Y. Tang, D. Lauretta, R.L. Ballouz, D. DellaGiustina, A. Polit, M. Westermann, C. Bennett, K. Becker, K. Walsh, D. Golish, Characterization and implications of a mass movement site in Bennu's Bralgha crater, *Icarus* **415**, 116056 (2024).
- [49] R.L. Ballouz, H. Agrusa, O. Barnouin, K. Walsh, Y. Zhang, R. Binzel, V. Bray, D. DellaGiustina, E. Jawin, J. DeMartini et al., Shaking and tumbling: Short-and long-timescale mechanisms for resurfacing of near-earth asteroid surfaces from planetary tides and predictions for the 2029 Earth encounter by (99942) Apophis, *Planet. Sci. J.* **5**, 251 (2024).
- [50] E. Jawin, T. McCoy, K. Walsh, H. Connolly Jr, R.L. Ballouz, A. Ryan, H. Kaplan, M. Pajola, V. Hamilton, O. Barnouin et al., Global geologic map of asteroid (101955) Bennu indicates heterogeneous resurfacing in the past 500,000 years, *Icarus* **381**, 114992 (2022).
- [51] B. Cheng, Y. Yu, E. Asphaug, P. Michel, D.C. Richardson, M. Hirabayashi, M. Yoshikawa, H. Baoyin, Reconstructing the formation history of top-shaped asteroids from the surface boulder distribution, *Nat. Astron.* **5**, 134 (2021).
- [52] Y. Zhang, P. Michel, O.S. Barnouin, J.H. Roberts, M.G. Daly, R.L. Ballouz, K.J. Walsh, D.C. Richardson, C.M. Hartzell, D.S. Lauretta, Inferring interiors and structural history of top-shaped asteroids from external properties of asteroid (101955) Bennu, *Nat. Commun.* **13**, 4589 (2022).
- [53] K. Ishimaru, D. Lauretta, Analysis of layered boulders on asteroid (101955) Bennu and their implications for fluid flow on the parent body, *Meteorit. Planet. Sci.* **59**, 193 (2024).
- [54] K.A. Holsapple, Main belt asteroid collision histories: Cratering, ejecta, erosion, catastrophic dispersions, spins, binaries, tops, and wobblers, *Planet. Space Sci.* **219**, 105529 (2022).
- [55] W.F. Bottke Jr., M.C. Nolan, R. Greenberg, R.A. Kolvoord, Velocity distributions among colliding asteroids, *Icarus* **107**, 255 (1994).
- [56] W.F. Chen, D.J. Han, *Plasticity for Structural Engineers* (Springer-Verlag, New York, 1988)
- [57] M. Arakawa, and 67 others, An artificial impact on the asteroid (162173) Ryugu formed a crater in the gravity-dominated regime, *Science* **368**, 67 (2020).
- [58] S.B. Savage, K. Hutter, The motion of a finite mass of granular material down a rough incline, *J. Fluid Mech.* **199**, 177 (1989).
- [59] J. Gray, M. Wieland, K. Hutter, Gravity-driven free surface flow of granular avalanches over complex basal topography, *Proc. R. Soc. A* **455**, 1841 (1999).
- [60] K. Gaurav, D. Banik, I. Sharma, Coupled shape and spin evolution of small near spherical asteroids due to global regolith motion (2025), <https://arxiv.org/abs/2505.18960>
- [61] M. Cooper, R. Kovach, J. Watkins, Lunar near-surface structure, *Rev. Geophys.* **12**, 291 (1974).
- [62] J. Goddard, Nonlinear elasticity and pressure-dependent wave speeds in granular media, *Proc. R. Soc. A* **430**, 105 (1990).
- [63] M. Nolan, E. Howell, D. Scheeres, J. McMahon, O. Golubov, C. Hergenrother, J. Emery, K. Noll, S. Chesley, D. Lauretta, Detection of rotational acceleration of Bennu using HST light curve observations, *Geophys. Res. Lett.* **46**, 1956 (2019).